MEMOIRS OF THE COLLEGE OF SCIENCE, UNIVERSITY OF KYOTO, SERIES B,
Vol. XXIV, No. 2 Geology and Mineralogy, Article 1, 1957

Studies on the Metamictization of Radioactive Minerals

By

Tateo UEDA

Geological and Mineralogical Institute, University of Kyoto

(Received June 29, 1957)

Abstract

Radioactive minerals are melted, portion by portion, by the irradiation arising from disintegration of the radioactive elements contained in these minerals. The melted portion solidifies later on. The solidification occurres in two ways. One is that taking place in an original crystalline phase and in this case metamictization does not proceed, the other is that not doing and in this case metamictization proceeds.

Introduction

Most of radioactive minerals are in the course of time transformed into a metamict state. In a metamict state lattices are broken down and the minerals are amorphous, retaining their crystal forms. As the agent causing the metamict state is accepted the irradiation arising from disintegration of the radioactive elements contained in the minerals. Since, however, certain radioactive minerals have not been found in an amorphous state, there must be another agent in the metamictization. Recently, much of the interest in irradiation effects has been aroused by the increasing need for shielding materials suitable for the applications of nuclear science. However, as KINCHIN and PEASE (1955) say, it is not understood why the metamict state appears in some radioactive minerals and not in others.

MÜGGE (1922), FAESSLER (1942), HUTTON (1950), PABST (1951) and HURLEY and FAIRBAIRN (1953) pointed out several radioactive minerals as being always crystalline, which are tabulated in Table 1.

Minerals whose one of principal chemical constituents is such elements as *Cb*, *Ta*, *Ti* and *rare earth* frequently bear radioactive elements in substitution for these elements. This is, however, not always the case. Among the minerals tabulated in Table 1 certain minerals are very doubtful to be treated as radioactive minerals. However, monazite, xenotime, thorianite and huttonite can be treated for a certainty as radioactive minerals, excluding secondary minerals. Autunite, carnotite, gummite, metatorbernite, tyuyamunite and uvanite are of secondary origin. Since these minerals are those which crystallized at the surface of the earth, it is not difficult to understand that the lattices of these minerals, when broken down, are immedi-

Table 1. Radioactive minerals which are said to be always crystalline.

Author	Mineral	Chemical composition
MÜGGE	monazite	$(Ce, Th)PO_4$
	xenotime	$(Y, U)PO_4$
FAESSLER	thortveitite	$(Sc, Y)_2Si_2O_7$
	columbite	$(Fe, Mn)(Cb, Ta)_2O_6$
	stibiotantalite	$Sb(Ta, Cb)O_4$
	xenotime	$(Y, U)PO_4$
	monazite	$(Ce, Th)PO_4$
	thorianite	ThO_2
	yttrofluorite	Ca_3YF_9
	bastnaesite	$(Ce, La)(CO_3)F$
HUTTON	xenotime	$(Y, U)PO_4$
	monazite	$(Ce, Th)PO_4$
	thorianite	ThO_2
PABST	huttonite	$ThSiO_4$
HURLEY and FAIRBAIRN	monazite	$(Ce, Th)PO_4$
	autunite	$Ca(UO_2)_2(PO_4)_2 \cdot 10\text{-}12H_2O$
	carnotite	$K_2(UO_2)_2(VO_4)_2 \cdot 3H_2O$
	gummite	$UO_3 \cdot nH_2O$
	metatorbernite	$Cu(UO_2)_2(PO_4)_2 \cdot 8H_2O$
	tyuyamunite	$Ca(UO_2)_2(VO_4)_2 \cdot nH_2O$
	uvanite	$U_2V_6O_{21} \cdot 15H_2O$

ately restored under the same environment. In this paper secondary minerals are not taken into consideration.

VEGARD (1927) proved by X-ray powder photographing that some specimen of xenotime was slightly metamict, and later KARKHANAVARA and SHANKAR (1954) and the author (1955) independently proved by the same method that some specimen of monazite was also slightly metamict. However, no one has ever found these minerals in a fully amorphous state.

Results obtained by previous authors in the studies on the metamictization can be summarized as follows:

1) With progress of the metamictization, radioactive minerals decrease in refringence and birefringence and finally become isotropic optically, and in accordance with such change they become weak and diffuse in an X-ray diffraction and finally give no diffraction, however, in zircon the ultimate product of the metamictization is in some case an aggregate of crystalline ZrO_2 and amorphous SiO_2 as observed by VON STACKELBERG and CHUDOBA (1937) and BAUER (1939).

2) With progress of the metamictization, radioactive minerals decrease in density, although there are observations made by VON STACKELBERG and CHUDOBA, BAUER, and HURLEY and FAIRBAIRN that there was no direct relationship between density and the degree of the metamictization.

3) Being heated, radioactive minerals in the metamict state become anisotropic optically or increase in refringence and birefringence accompanied with increase in density, and in accordance with such change they give an X-ray diffraction or become strong and sharp in an X-ray diffraction.

4) In the course of the metamictization, lattice distension takes place as observed by the author (1954) in allanite and by HOLLAND and GOTTFRIED (1955) in zircon.

In the present study the author clarify why the metamict state appears in some radioactive minerals and not in others, dealing with zircon, allanite, gadolinite, monazite and xenotime owing to the availability of the results of structure analyses.

I. Process of the metamictization

Zircon, allanite, monazite and xenotime were examined by means of X-ray powder method, using Norelco Geiger counter X-ray spectrometer of North American Philips Co. The spectrometer was worked with following conditions.

Voltage: 30 kV
Current: 15 mA
Radiation: Cu-K_α
Scanning speed: 1° per minute
Chart speed: 1/2 inch per minute
Scale factor: 4 or 8
Multiplier: 1
Time constant: 8 second
Slits: 1°-0.006″-1°

Pulverization of specimens was carefully carried out so that the powders of the specimens might not differ in size with different specimens. Packing of the powders into the hollow of glass plate was also carefully so that the powders might not differ in compactness with different specimens. 2θ angles were measured at the maxima of diffraction peaks and calibrated by silicon diffraction pattern using the method of least squares.

1. Zircon

Specimens submitted to the present examination are as follows.

	Locality	Specific gravity
A.	Burma	4.66
B.	Omiya-chô (Morimoto), Kyoto Pref.	4.40
C.	Hagata-mura, Ehime Pref.	4.38
D.	Mineyama-chô (Oro), Kyoto Pref.	4.24

E.	Omiya-chô (Kôbe), Kyoto Pref.	4.21
F.	Yamaguchi-mura, Nagano Pref.	4.20
G.	Ishikawa-chô (Ishikawa), Fukushima Pref.	4.18
H.	Otsu-shi (Shimotanakami), Shiga Pref.	4.18
I.	Nakatsugawa-shi (Naegi), Gifu Pref.	4.24

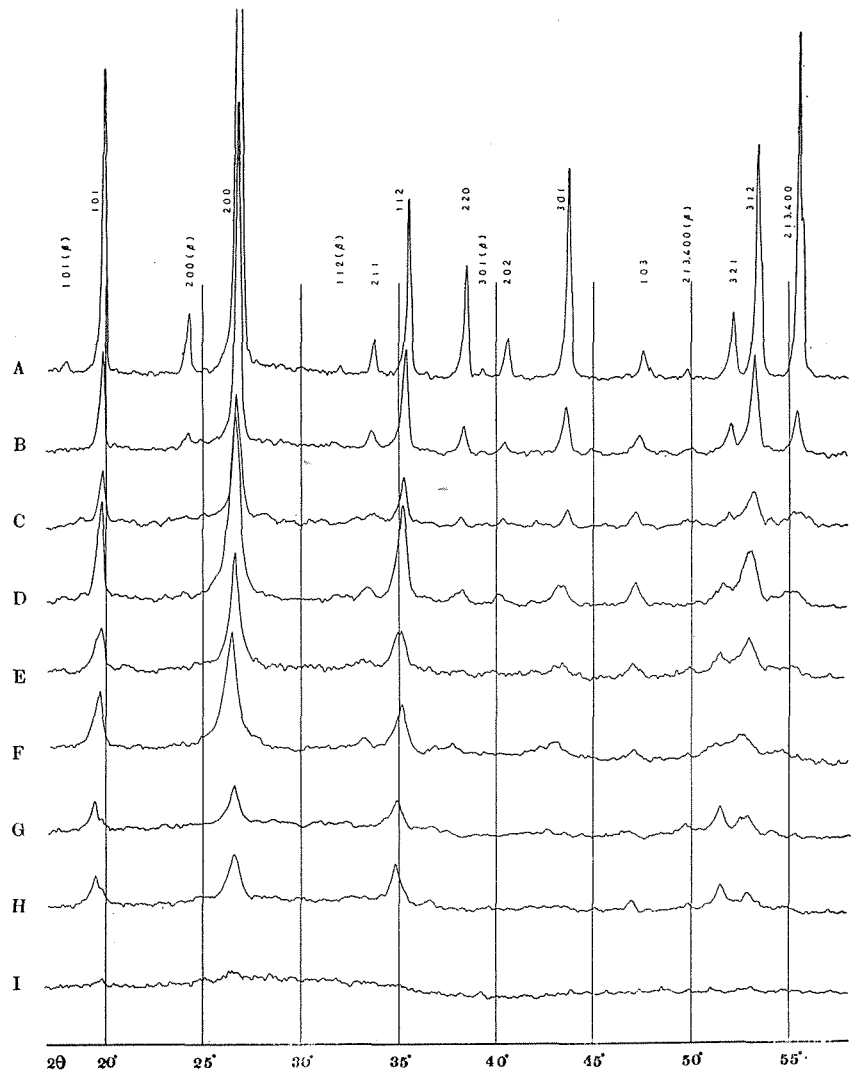

Fig. 1. Diffraction patterns of zircon, showing the range from 17° to 58° (2θ). A, B, C, D, E, F, G, H, I denote the localities of the specimens described above.

Specific gravity was measured by means of pycnometer method. Diffraction patterns of these specimens are arranged in Fig. 1, however, only in the range from 17° to 58° (2θ). As will be seen in Fig. 1, peaks in the diffraction patterns are, on the whole, symmetrical in shape. In some specimens, however, peaks were asymmetrical in shape and frequently branched off into branchlets. In the present examination measurement with such patterns was abandoned.

Comparing the diffraction patterns shown in Fig. 1 with one another, the following are noticeable. (1) Peaks decrease progressively in sharpness and in height and finally fade away as density decreases. (2) Peaks shift more and more towards low angle side as they decrease in sharpness and in height. Hence, it follows that transformation into a metamict state arises from gradual lattice disordering and the disordering is accompanied with lattice distension. Indices of the reflexions which brought forth these peaks were calculated making use of the result of structure analysis with zircon (specific gravity, 4.70), carried out by VEGARD (1926). In Table 2 are shown the indices of the reflexions and their $\sin^2\theta$–values.

Table 2. $\sin^2\theta$–values of the reflexions in the diffraction patterns of zircon.

hkl	$\sin^2\theta$							
	A	B	C	D	E	F	G	H
101	.03024	.03006	.03005	.02976	.02966	.02946	.02887	.02887
200	.05438	.05436	.05397	.05357	.05357	.05266	.05344	.05344
211	.08468	.08419	.08434	.08321		.08209		
112	.09364	.09278	.09243	.09210	.09110	.09160	.08976	.08976
220	.10903	.10833	.10707	.10725		.10528		
202	.12076	.11961	.11942	.11829				
301	.13935	.13832	.13852	.13672	.13691	.13452		
103	.16305	.16135	.16050	.16006	.15922	.15986	.15834	.15836
321	.19378	.19262	.19171	.18988	.18875	.18760	.18920	.18920
312	.20259	.20119	.20049	.19933	.19909	.19654	.19770	.19909
{213 {400	.21800	.21679	.21583	.21368		.21060		

A, B, C, D, E, F, G, H denote the localities of the specimens described before.

Cell-dimensions of the specimens were calculated from the $\sin^2\theta$–values by the following equation using the method of least squares.

$$4\sin^2\theta = h^2 a_1^{*2} + k^2 a_2^{*2} + l^2 c^{*2}$$

Results are shown in Table 3 in which cell-dimensions determined by VEGARD are inserted for comparison.

Now, it is clear that cell-dimensions increase progressively as the disordering proceeds, that is, as the metamictization proceeds, and that the lattice distension takes

Table 3. Cell-dimensions, rates of increase of the cell-dimensions, cell-volumes and reciprocal cell-volumes of zircon.

	VEGARD	A	B	C	D	E	F	G	H
a_1	6.59 Å	6.600	6.620	6.616	6.660	6.645	6.717	6.657	6.623
		(0.15%)	(0.46)	(0.39)	(1.06)	(0.83)	(1.93)	(1.02)	(0.50)
a_2	6.59 Å	6.595	6.612	6.678	6.658	6.776	6.704	6.730	6.803
		(0.08%)	(0.33)	(1.34)	(1.03)	(2.82)	(1.73)	(2.12)	(3.23)
c	5.94 Å	5.974	6.001	6.016	6.032	6.048	6.049	6.080	6.078
		(0.57%)	(1.03)	(1.28)	(1.55)	(1.82)	(1.84)	(2.36)	(2.32)
V	257.96 Å^3	260.03	262.67	265.80	267.47	272.32	272.39	272.39	273.85
$\frac{1}{V}\times 10^3$	3.877	3.846	3.807	3.762	3.739	3.672	3.671	3.671	3.652

A, B, C, D, E, F, G, H denote the localities of the specimens described before.

place anisotropically. The rates of increase of a_1, a_2 and c, compared with the cell-dimensions determined by VEGARD are shown in the parentheses in Table 3. Occurrence of the asymmetrical peaks may be due to unequality of the degree of the metamictization within a crystal and the unequality may be ascribed to intensely inhomogeneous distribution of the radioactive elements within the crystal.

Comparing the cell-volumes in Table 3 with one another, it follows that cell-volume increases with decreasing density. In Fig. 2 are plotted densities against reciprocal cell-volumes. The slope of line A denotes the proportional constant in a case where the decrease of density is due only to the increase of cell-volume. The slope is obtainable by calculating as follows:

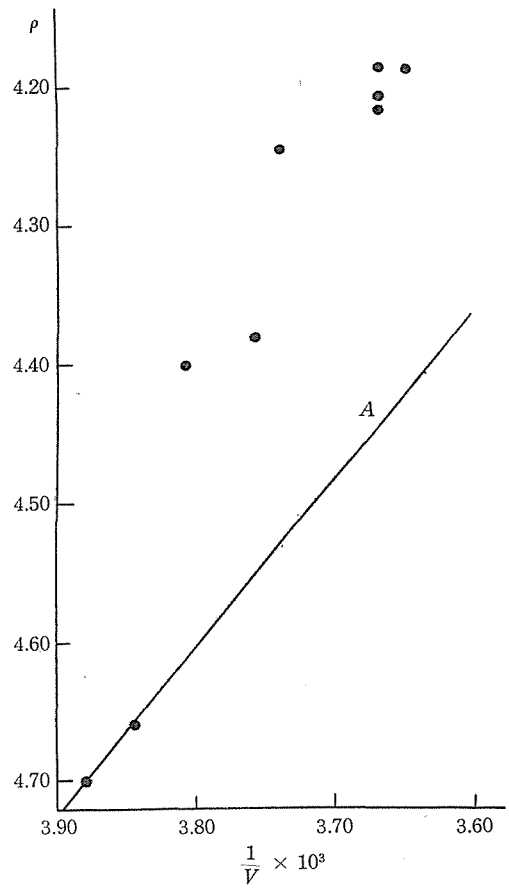

Fig. 2. Relation between reciprocal cell-volumes and densities of zircon.

$$\rho = \frac{Z \times \text{Molecular weight}}{\text{Avogadro's number} \times V}$$
$$= \frac{4 \times 183.28}{6.02402 \times 10^{23} \times V \times 10^{-24}}$$
$$= 1.217 \times \left(\frac{1}{V} \times 10^{3}\right)$$
$$= \tan 50°35' \times \left(\frac{1}{V} \times 10^{3}\right)$$

where, ρ: density, Z: number of molecules in a unit cell,
V: cell-volume.

The plotted points deviate considerably from the line A as will be seen in Fig. 2, that is, the rate of decrease of density is by far greater, compared with that of increase of cell-volume.

2. Allanite

Specimens submitted to the present examination are as follows.

	Locality	Specific gravity
A.	Anag-ub, Whanghe-do, Korea	4.08
B.	Kyoto-shi (Daimonji-yama), Kyoto Pref.	3.85
C.	Omiya-chô (Morimoto), Kyoto Pref.	3.88
D.	Oyama-chô, Toyama Pref.	3.85
E.	Hagsong-myon, Hamgyongbug-do, Korea	3.85
F.	Shiga-chô (Kido), Shiga Pref.	3.84
G.	Hagata-mura, Ehime Pref.	3.82
H.	Tungwenchungtan, North China	3.70
I.	Kawamata-chô (Kojima), Fukushima Pref.	3.79
J.	Santaikou, South Manchuria	3.61
K.	Tafangshen, South Manchuria	3.66
L.	Ishikawa-chô (Nogizawa), Fukushima Pref.	3.65

Specific gravity was measured by means of pycnometer method. Diffraction patterns of these specimens are arranged in Fig. 3, however, only in the range from 20° to 50° (2θ). As will be seen in Fig. 3, peaks in the diffraction patterns are, on the whole, symmetrical in shape. In some specimens, however, peaks were extremely asymmetrical and frequently branched off into branchlets as in some specimens of zircon. Measurement with such patterns was abandoned.

Comparing the diffraction patterns shown in Fig. 3 with one another, the same is observed as in the case of zircon. (1) Peaks decrease progressively in sharpness and in height and finally fade away as density decreases. (2) Peaks shift more and more towards low angle side as they decrease in sharpness and in height.

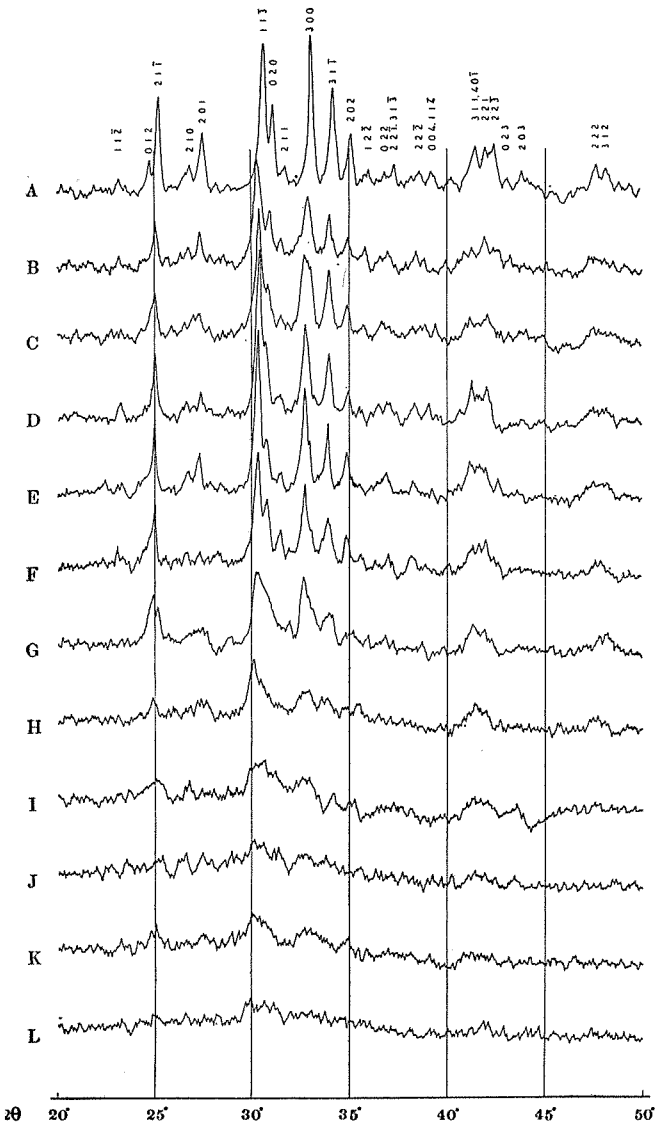

Fig. 3. Diffraction patterns of allanite, showing the range from 20° to 50° (2θ). A, B, C, D, E, F, G, H, I, J, K, L denote the localities of the specimens described above.

Indices of the reflexions which brought forth these peaks were calculated making use of the result of structure analysis carried out by the author (1955). In Table 4 are shown the indices of the reflexions and their $\sin^2\theta$-values. Cell-dimensions of

Table 4. $\sin^2\theta$-values of the reflexions in the diffraction patterns of allanite.

hkl	$\sin^2\theta$							
	A	B	C	D	E	F	G	H
001	.00704	.00697	.00694	.00695				
100	.00903	.00902	.00902	.00885	.00873			
101	.02262	.02245	.02250	.02244	.02246	.02236		.02233
011			.02474					
110	.02693	.02678	.02657	.02654	.02648	.02651	.02644	
$11\bar{2}$	.04056	.04088		.04056		.03996		
012	.04601							
$21\bar{1}$	.04783	.04722	.04735	.04696	.04709	.04696	.04674	.04661
210	.05396	.05368		.05318	.05338	.05318		
201	.05664	.05607	.05636	.05607	.05598	.05598	.05555	.05541
$11\bar{3}$	.06991	.06875	.06906	.06906	.06859	.06859	.06852	.06755
020	.07204	.07129	.07097	.07038	.07054	.07065	.07023	.06917
211	.07475	.07382	.07398	.07355	.07382	.07382	.07382	.07322
300	.08100	.08049	.08020	.07986	.07958	.07958	.07941	
$31\bar{1}$	.08661	.08561	.08561	.08550	.08532	.08515	.08532	.08497
202	.09108	.09024	.09024	.09042	.08976	.08976	.08958	.08827
$12\bar{2}$	.09567	.09462	.09462			.09364		
022	.09998	.09878	.09948					
$\begin{cases}22\bar{1}\\31\bar{3}\end{cases}$	.10246	.10106		.10106	.10036	.10068		
$22\bar{2}$	.10943	.10850		.10831	.10758	.10726		
$\begin{cases}004\\11\bar{4}\end{cases}$	.11269			.11182				
$\begin{cases}311\\40\bar{1}\end{cases}$	.12574	.12419	.12397	.12440	.12376		.12375	
221	.12859	.12845	.12631	.12631	.12709			.12553
$22\bar{3}$	.13133		.12924	.12881	.12859	.12859	.12855	
023	.13513							
203	.13950							
222	.16273		.16265					
312	.16655							
$13\bar{2}$	.18827							
$23\bar{1}$	.19149							
303	.20494							
231	.21996	.21585						
313	.22278							

A, B, C, D, E F, G, H denote the localities of the specimens described before.

Table 5. Cell-dimensions, cell-volumes and reciprocal cell-volumes of allanite.

	A	B	C	D	E	F	G	H
a	8.929 Å	8.981	8.978	8.986	9.010	9.011	9.019	8.970
b	5.736 Å	5.770	5.779	5.804	5.791	5.790	5.802	5.853
c	10.147 Å	10.243	10.206	10.182	10.251	10.243	10.257	10.327
β	114°54′	115°04′	115°00′	114°56′	115°08′	115°04′	115°08′	114°40′
V	471.41 Å^3	480.79	479.90	481.55	484.24	484.06	485.91	492.72
$\frac{1}{V}\times 10^3$	2.121	2.080	2.084	2.077	2.065	2.066	2.058	2.030

A, B, C, D, E, F, G, H denote the localities of the specimens described before.

the specimens were calculated from the $\sin^2\theta$-values, selecting $21\bar{1}$, 201, $11\bar{3}$, 020, 211, 300, $31\bar{1}$, 202 reflexions, by the following equation using the method of least squares.

$$4\sin^2\theta = h^2a^{*2}+k^2b^{*2}+l^2c^{*2} +2hla^*c^*\cos\beta^*$$

Results are shown in Table 5. Comparing the values in Table 5, it follows, as in the case of zircon, that cell-dimensions increase progressively as the disordering proceeds, that is, as the metamictization proceeds, and that cell-volume increases with decreasing density. However, the rate of decrease of density is by far greater, compared with that of increase of the cell-volume. In Fig. 4 are plotted densities against reciprocal cell-volumes, where line A bears the same meaning as in Fig. 2. The relationship between the reciprocal cell-volumes and the densities is the same as in zircon. Hence, it follows that the process of the metamictization in allanite is the same as in zircon.

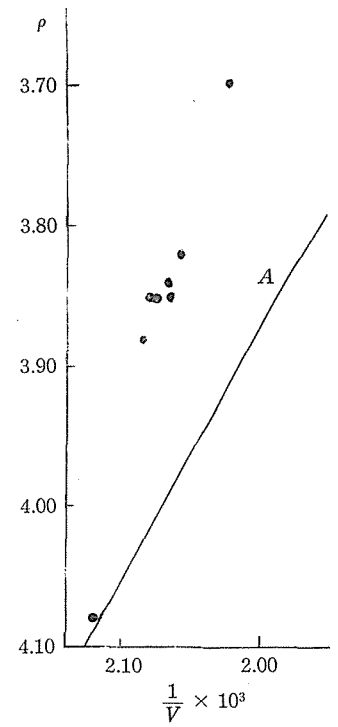

Fig. 4. Relation between reciprocal cell-volumes and densities of allanite.

3. Monazite

Specimens submitted to the present examination are as follows.

	Locality	Specific gravity
A.	Tôwa-mura (Harimichi), Fukushima Pref.	5.20
B.	Ishikawa-chô (Nogizawa), Fukushima Pref.	5.16
C.	Begyang-myon, Pyonganbug-do, Korea	5.11
D.	Omiya-chô (Kôbe), Kyoto Pref.	5.12
E.	Sunan-ub, Pyongannam-do, Korea	5.08
F.	India	5.33

Specific gravity was measured by means of pycnometer method. Diffraction patterns of these specimens are arranged in Fig. 5, however, only in the range from 15° to 56° (2θ). As will be seen in Fig. 5, peaks in the diffraction patterns are symmetrical in shape. Asymmetrical peaks were not observed so far as specimens examined were concerned.

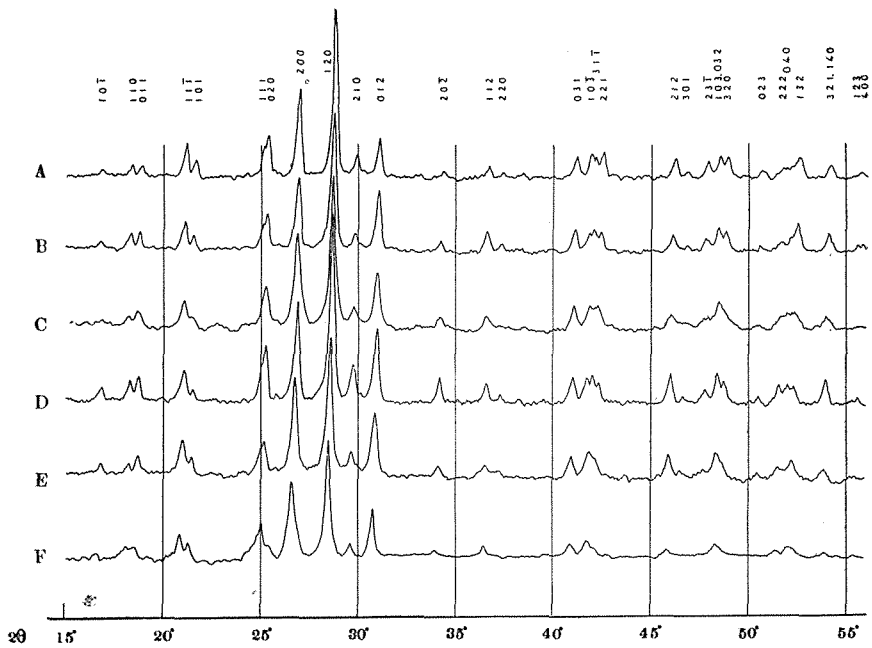

Fig. 5. Diffraction patterns of monazite, showing the range from 15° to 56° (2θ). A, B, C, D, E, F denote the localities of the specimens described above.

Comparing the diffraction patterns shown in Fig. 5 with one another, the following are noticeable. (1) Peaks make no remarkable difference in sharpness and in height between the specimens. (2) Peaks shift more and more, although not so remarkable, towards low angle side as density decreases, however, with an exception of the specimen from India. Indices of the reflexions which brought forth these peaks were calculated making use of the result of structure analysis carried out by

the author (1953). In Table 6 are shown the indices of the reflexions and their $\sin^2\theta$-values. Cell-dimensions of the specimens were calculated from the $\sin^2\theta$-values, selecting 200, 120, 012, 20$\bar{2}$ 112 031, 212, 132 reflexions, by the following equation using the method of least squares.

Table 6. $\sin^2\theta$-values of the reflexions in the diffraction patterns of monazite.

hkl	$\sin^2\theta$					
	A	B	C	D	E	F
10$\bar{1}$	.02176	.02173	.02167	.02143	.02167	.02143
110	.02576	.02582	.02547	.02538	.02547	.02528
011	.02716	.02706	.02686	.02657	.02686	.02657
11$\bar{1}$	.03404	.03393	.03375	.03342	.03364	.03364
101	.03553	.03542	.03501	.03489	.03501	.03501
111	.04783	.04770			.04709	.04709
020	.04858	.04844	.04809	.04796	.04796	.04783
200	.05476	.05476	.05424	.05424	.05424	.05396
120	.06225	.06215	.06170	.06155	.06155	.06140
210	.06682	.06682	.06600	.06625	.06584	.06584
012	.07215	.07204	.07172	.07129	.07156	.07156
20$\bar{2}$	.08779	.08726	.08714	.08661	.08644	.08579
112	.09960	.09948	.09878	.09841	.09841	.09860
220	.10330	.10317	.10208	.10227	.10208	
031	.12419	.12419	.12306	.12285	.12243	.12285
10$\bar{3}$	.12960	.12824	.12802	.12709	.12745	.12745
31$\bar{1}$	.12996	.12960	.12960	.12859	.12802	
221	.13257	.13177	.13018	.13061	.12996	.12996
212	.15437	.15374	.15249	.15265	.15187	.15249
301	.15872	.15832		.15705	.15563	
23$\bar{1}$	.16524	.16459	.16370	.16370	.16305	
{103 {032	.16933	.16892	.16826	.16785	.16720	.16826
320	.17223	.17173		.17024	.16933	
023	.18378	.18284		.18199	.18148	
222	.19079	.19053	.18940	.18923	.18896	
040		.19378	.19176	.19219		
132	.19705	.19607	.19378	.19448	.19448	.19404
{321 {140	.20821	.20748	.20539	.20584	.20566	.20521
123	.21940	.21753		.21725		
400		.21874				

A, B, C, D, E, F denote the localities of the specimens described before.

Table 7. Cell-dimensions, cell-volumes, reciprocal cell-volumes and ThO_2 contents of monazite.

	A	B	C	D	E	F
a	6.774 Å	6.785	6.804	6.809	6.825	6.845
b	6.989 Å	6.996	7.037	7.030	7.041	7.033
c	6.465 Å	6.481	6.489	6.511	6.506	6.513
β	103°44′	103°45′	103°31′	103°47′	103°41′	104°00′
V	297.31 $Å^3$	298.83	302.07	302.68	303.78	304.23
$\frac{1}{V}\times 10^3$	3.363	3.346	3.310	3.304	3.292	3.287
ThO_2	11.73%	10.01	9.96	12.02	9.68	15.00

A, B, C, D, E, F denote the localities of the specimens described before.

$$4\sin^2\theta = h^2a^{*2}+k^2b^{*2}+l^2c^{*2} +2hla^*c^*\cos\beta^*$$

Results are shown in Table 7.

Now, it is appreciable that cell-volume increases with decreasing density, provided that specimens are much the same in ThO_2-content. At the bottom in Table 7 are inserted ThO_2-contents of the specimens, which were determined by the author. The high density of the specimen from India, notwithstanding its large cell-volume, is probably due to the high content of ThO_2. In Fig. 6 are plotted densities against reciprocal cell-volumes, where line A bears the same meaning as in Fig. 2 and Fig. 4. The plotted points are approximately located on the line A. Hence, it follows that the effect of irradiation on monazite is different from that on zircon and on allanite. One point far from the line A is that due to the specimen from India.

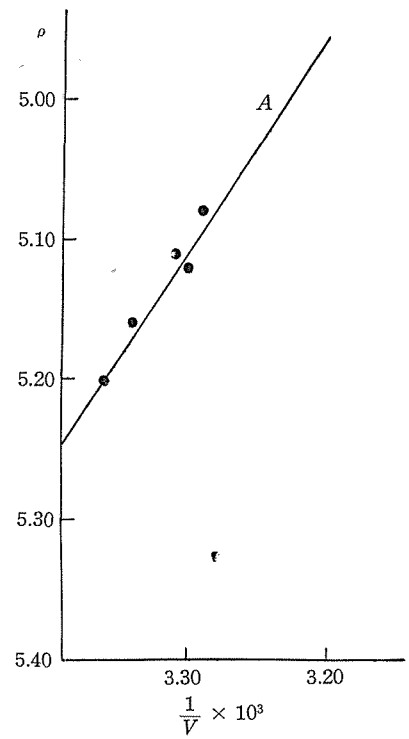

Fig. 6. Relation between reciprocal cell-volumes and densities of monazite.

4. Xenotime

It was difficult for the author to get specimens of xenotime from different localities and those from only two localities were submitted to the present examination. These are as follows.

	Locality	Specific gravity
A.	Norway	4.70
B.	Ishikawa-chô (Ishikawa), Fukushima Pref.	4.63

Specific gravity was measured by means of pycnometer method. Diffraction patterns of these specimens are arranged in Fig. 7, however, only in the range from 16° to 56° (2θ). Comparing these two patterns, it can be understood that lattice distension takes place in xenotime, too. Indices of the reflexions which brought about peaks in the diffraction patterns were calculated making use of the result of structure analysis carried out by VEGARD (1927). In Table 8 are shown the indices of the reflexions and their $\sin^2\theta$–values. Cell-dimensions of the specimens were

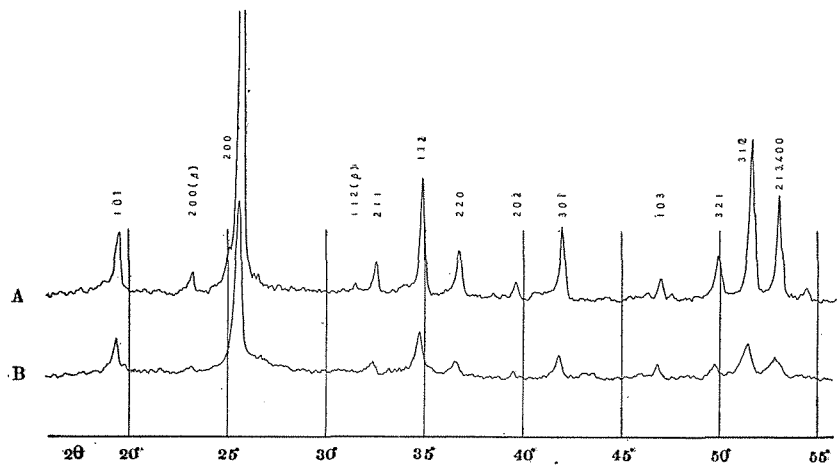

Fig. 7. Diffraction patterns of xenotime, showing the range from 16° to 56° (2θ). A, B denote the localities of the specimens described above.

Table 8. $\sin^2\theta$–values of the reflexions in the diffraction patterns of xenotime.

hkl	$\sin^2\theta$		*hkl*	$\sin^2\theta$	
	A	B		A	B
101	.02887	.02859	301	.12859	.12824
200	.05009	.04986	103	.15920	.15896
211	.07879	.07846	321	.17842	.17792
112	.09024	.08976	312	.18992	.18923
220	.09979	.09891	{213 {400	.19954	.19909
202	.11512	.11492			

A, B denote the localities of the specimens described before.

calculated from the $\sin^2\theta$-values by the following equation using the method of least squares.

$$4\sin^2\theta = h^2 a_1^{*2} + k^2 a_2^{*2} + l^2 c^{*2}$$

Results are shown in Table 9, in which cell-dimensions determined by VEGARD were inserted for comparison.

Table 9. Cell-dimensions and cell-volumes of xenotime.

	VEGARD	A	B
a_1	6.89 Å	6.873	6.882
a_2	6.89 Å	6.944	6.980
c	6.04 Å	6.114	6.120
V	286.73 Å^3	291.80	293.98

A, B denote the localities of the specimens described before.

VEGARD gave no description of the density of the specimen submitted to structure analysis, and data obtained in the present examination is scanty. Hence, no further investigation.

II. Consideration to the process of the metamictization

In the process of the metamictization, the increase of cell-volume and the decrease of density take place, and in monazite the decrease of density is inversely proportional to the increase of cell-volume, in zircon and in allanite, however, such relationship is not maintained, that is, the rate of decrease of density is by far greater, compared with the rate of increase of cell-volume.

According to VON STACKELBERG and CHUDOBA (1937) who examined zircon especially low in density, upon the X-ray rotation photographs one specimen whose density was 3.972 gave cubic ZrO_2 Debye-rings together with a very weak single crystal pattern of zircon, being heated to 640°C, together with a somewhat strong single crystal pattern of the same; another specimen whose density was 3.945 gave no diffraction, being heated to 640°C, weak cubic ZrO_2 Debye-rings; being heated to 1450°C both specimens gave single crystal zircon patterns, the latter was, however, somewhat disoriented. These results were later confirmed by BAUER (1939). VON STACKELBERG and CHUDOBA considered that zircon especially low in density consisted of ZrO_2 and SiO_2, where SiO_2 might be always amorphous and ZrO_2 crystalline or amorphous; and considered that the especially low density could be understood, taking into account that the densities of cubic ZrO_2 and amorphous SiO_2 are about 6.0 and about 2.2 respectively and the density of the equimolecular mixture of cubic ZrO_2 and amorphous SiO_2 is, therefore, about 3.9. The author considers that in zircon and in allanite decomposition may take place under the

influence of the irradiation arising from the disintegration of the radioactive elements contained in these minerals.

Many physicists have offered theoretical considerations concerning irradiation effect. According to SEITZ (1949), alpha-particle moving in a material heats up the material in the portion surrounding its track and displaces atoms at the end of its track by the collisions with them. According to SLATER (1951), alpha-particle passing through a material dissipates most of its energy by producing free electrons and excitons and the remaining energy is lost at the end of its travel by the collisions with atoms, producing interstitials and vacancies and generating heat. According to BRINKMAN (1954), during the time that alpha-particle holds high energy it displaces atoms, producing interstitials and vacancies and at the end of its travel it comes into collisions with atoms, generating heat. These considerations are different to some extent from one another. However, these physicists are in agreement with that the bombarding of alpha-particle and the recoiling of parent atom, which arise at the time when the radioactive decay takes place within a crystal, lead to the production of interstitials and vacancies as well as to the local generation of heat, which corresponds to exceedingly high temperature, within the crystal.

Basing on the present observations and that made by VON STACKELBERG and CHUDOBA and the theoretical considerations given by these physicists, the author considers that radioactive mineral in the earlier stage of the metamictization may consist of normal lattice portions and distended ones, brought about by the production of interstitials and vacancies, and melted portions, brought about by the generation of heat; with progress of the metamictization, normal lattice portions may decrease and distended portions and melted ones may increase, besides, in the distended portions, highly distended portions may become predominant; and in the later stage of the metamictization, radioactive mineral may consist mainly of the melted portions. In Fig. 8-A are illustrated these stages of the metamictization in which black circles denote the melted portions, dotted areaes the distended ones and the rest the normal ones. The melted portions may, in some case, take place decomposition and solidify in an amorphous phase or in crystalline phase (or phases) other than the original one, and in other case, may not take place decomposition and may solidify in the original crystalline phase. In the first case, the final stage of the metamictization must, of course, be amorphous. In the second case, it may also, in general, be amorphous X-ray diffractometrically as well as optically. For, the newly formed crystals may be randomly orientated and may be extremely minute on account of local melting and quenching. The author considers that in radioactive minerals which are sometimes amorphous (zircon, allanite, etc.), the melted portions may take place decomposition. In the third case, all the stages of the metamictization may be of the same crystalline

phase as the original one, although they may consist of normal lattice portions and distended ones. For, in such a case the orientation of recrystallized portion will be controlled by the ambient lattice surrounding it so that it grows again into the crystallographic orientation of parent crystal. The author considers that in radioactive minerals which have not been found in an amorphous state (monazite, xenotime, etc.), the melted portions may not take place decomposition and may recrystallize to the original crystalline state. In Fig. 8–B is illustrated such process of the metamictization, in which dotted areaes and the rest denote the same as in Fig. 8–A respectively.

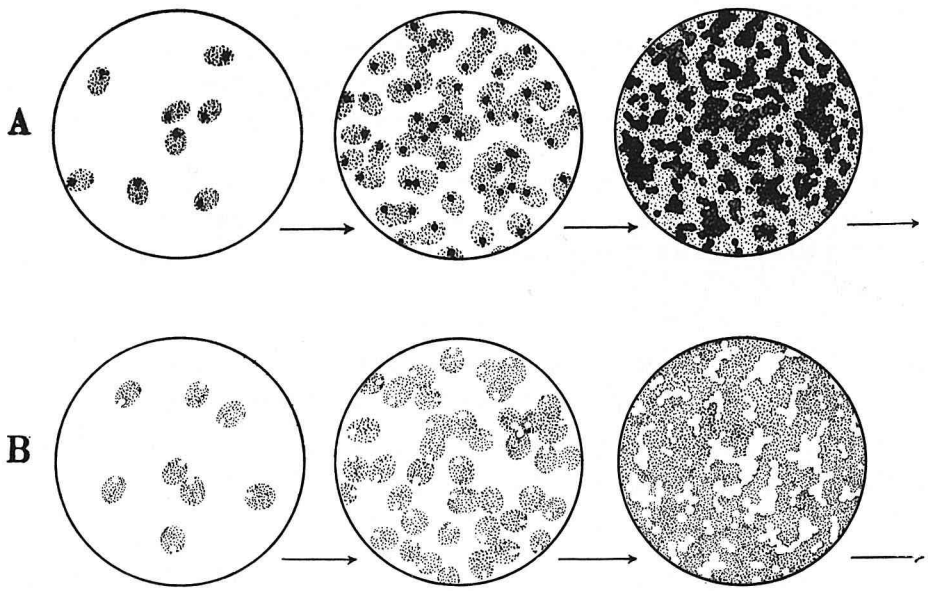

Fig. 8. Two types (supposed) of the process of the metamictization. Black circles, dotted areaes and the rest denote melted, distended and normal portions respectively.

Taking the process of the metamictization as above mentioned, it can be demonstrated convincingly that peaks in a diffraction pattern decrease in sharpness and in height and shift towards low angle side as the metamictization proceeds. For, when cell-dimensions are variable in a small range, peaks in a diffraction pattern must decrease in sharpness and in height, and therefore, must become diffuse, and peaks must become more diffuse as the range of variation of cell-dimensions become larger, and the maxima of peaks must shift towards low angle

side as the portions possessing larger cell-dimensions become predominant. The newly formed crystals may hardly affect on the diffraction pattern. For, even if they are in crystalline state, they may be expected to be extremely minute.

When a peak in a diffraction pattern is symmetrical in shape, the maximum of the peak gives a mean value of spacing. Accordingly, the cell-dimensions obtained in the present examination are the mean values of cell-dimensions in all the portions of a crystal.

If the process of the metamictization is such as said above, the same crystalline phase as the original one must precipitate in melting and then quenching radioactive minerals such as monazite, xenotime, etc., and amorphous phase or crystalline phase (or phases) other than the original one in so doing radioactive minerals such as zircon, allanite, etc.; and lattice contraction must take place in heating radioactive minerals, in which metamictization is in progress, at appropriate temperature and for appropriate duration. For, the distension of lattice has been considered to be due to the production of interstitials and vacancies.

In the following, first, will be examined the effect of heating on radioactive minerals in which metamictization is in progress, and next, will be inquired into what kind of phases will precipitate in melting and then quenching radioactive minerals.

III. Effect of heating on the radioactive minerals in which metamictization is in progress

Specimens in which metamictization is in progress were heated at 400°C and 800°C in vacuum (10^{-4} *mm Hg*) for two hours and quenched in air and then examined X-ray spectrometrically.

1. Zircon

Specimens from Burma and Mineyama-chô (Oro), Kyoto Pref. were submitted to the experiment. Diffraction patterns of the heated specimens together with those of the raw specimens for comparison are shown in Fig. 9, however, only in the range from 17° to 58° (2θ). As will be seen in Fig. 9, the effect of heating on the specimens comes in sight in the following respects:

a) Zircon from Burma.

Peaks somewhat decrease in height, but shift towards high angle side.

b) Zircon from Mineyama-chô (Oro).

Peaks increase in sharpness and in height, and shift towards high angle side.

In Table 10 are shown the $\sin^2\theta$–values of the reflexions of the heated specimens. Cell-dimensions and cell-volumes of the heated specimens were calculated from the $\sin^2\theta$–values in the same way described before. Results are shown in Table 11, in which cell-dimensions and cell-volumes of the raw specimens are inserted for comparison.

The results show that lattice contraction takes place by heating.

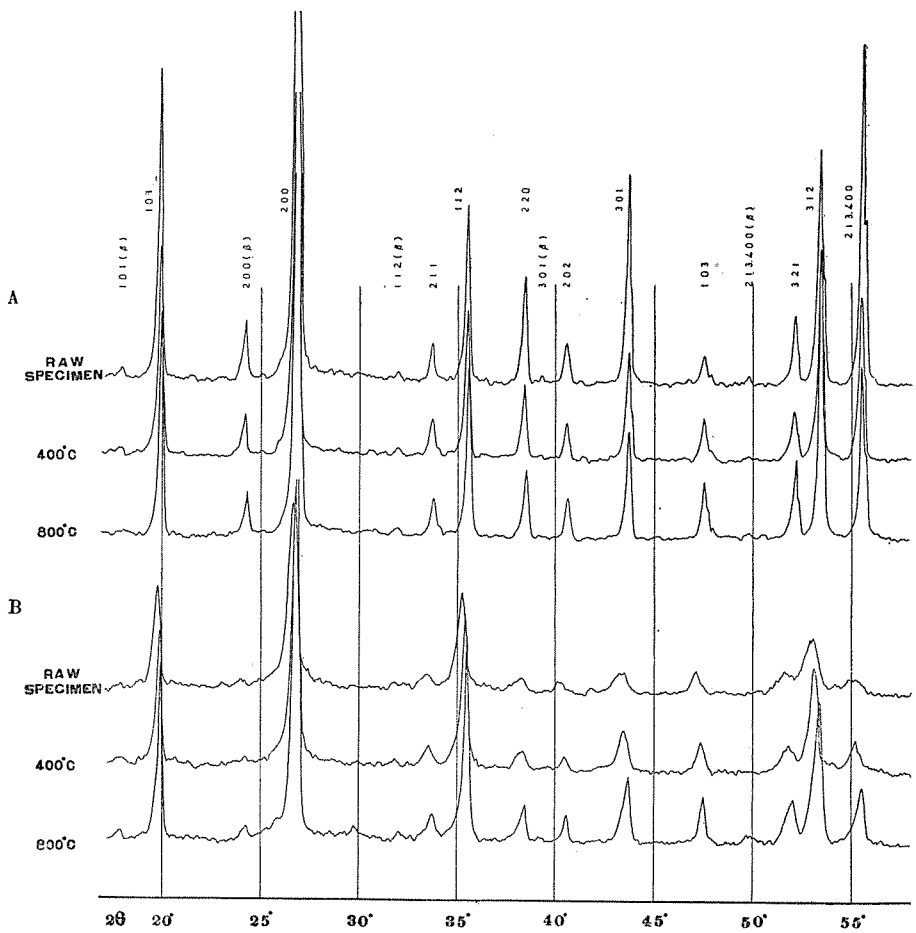

Fig. 9. Diffraction patterns of raw and heated specimens of zircon, showing the range from 17° to 58° (2θ).
A. From Burma. B. From Mineyama-chô (Oro).

Table 10. $\sin^2\theta$-values of the reflexions of heated specimens of zircon.

hkl	$\sin^2\theta$			
	From Burma		From Mineyama-chô (Oro)	
	400°C	800°C	400°C	800°C
101	.03035	.03035	.02996	.03017
200	.05438	.05448	.05373	.05438
211	.08486	.08486	.08352	.08433
112	.09376	.09394	.09260	.09327
220	.10903	.10943	.10758	.10850
202	.12110	.12110	.11944	.12034
301	.13935	.13935	.13712	.13876
103	.16330	.16330	.16112	.16201
321	.19351	.19378	.19149	.19237
312	.20286	.20286	.19981	.20142
{213 / 400	.21772	.21772	.21465	.21678

Table 11. Cell-dimensions and cell-volumes of raw and heated specimens of zircon.

		Raw specimen	Heated at 400°C	Heated at 800°C
From Burma	a_1	6.600 Å	6.597	6.598
	a_2	6.595 Å	6.592	6.585
	c	5.974 Å	5.973	5.973
	V	260.03 Å^3	259.75	259.51
From Mineyama-chô (Oro)	a_1	6.660 Å	6.649	6.614
	a_2	6.658 Å	6.626	6.625
	c	6.032 Å	6.015	5.993
	V	267.47 Å^3	265.00	262.60

2. Allanite

Specimens from Anag-ub, Whanghe-do, Korea; Omiya-chô (Morimoto), Kyoto Pref. and Kawamata-chô (Kojima), Fukushima Pref. were submitted to the experiment. Diffraction patterns of the heated specimens together with those of the raw specimens for comparison are shown in Fig. 10, however, only in the range from 20° to 50° (2θ). As will be seen in Fig. 10, the effect of heating on the specimens comes in sight in the following respects:

a) Allanite from Anag-ub.

Peaks somewhat increase in sharpness and in height, and shift towards high angle side.

b) Allanite from Omiya-chô (Morimoto)
Peaks somewhat increase in sharpness and shift towards high angle side.
c) Allanite from Kawamata-chô (Kojima)
Peaks increase in sharpness and in height, and shift towards high angle side.

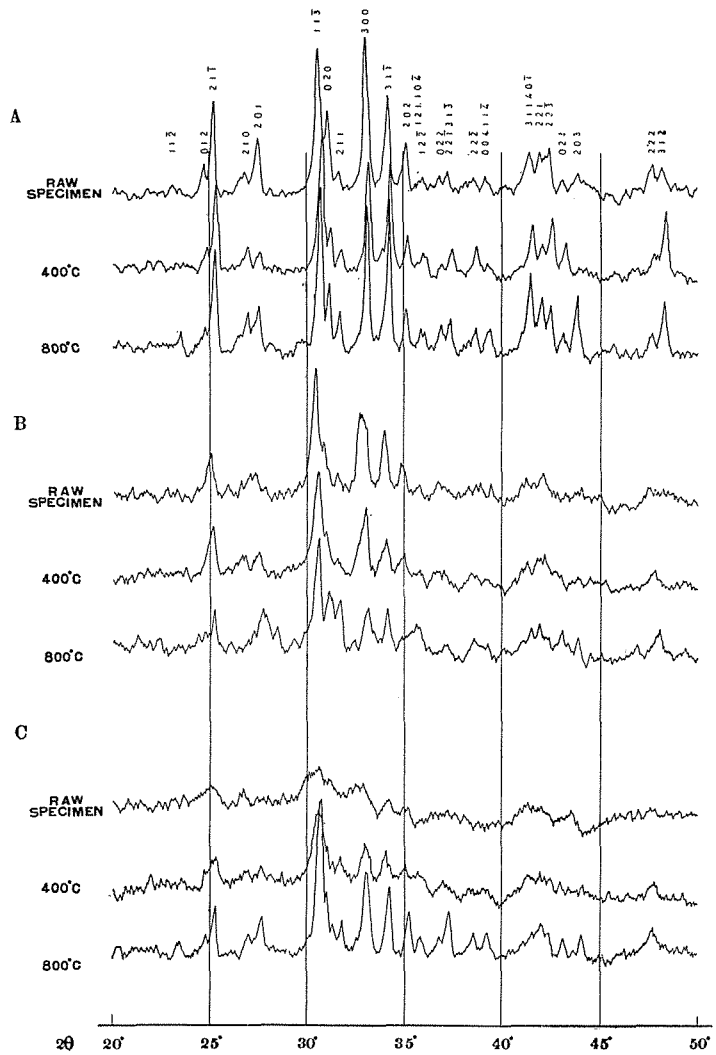

Fig. 10. Diffraction patterns of raw and heated specimens of allanite, showing the range from 20° to 50° (2θ).
A. From Anag-ub. B. From Omiya-chô (Morimoto).
C. From Kawamata-chô (Kojima).

In Table 12 are shown the $\sin^2\theta$-values of the reflexions of the heated specimens. Cell-dimensions and cell-volumes of the heated specimens were calculated from the $\sin^2\theta$-values, selecting $21\bar{1}$, 201, $11\bar{3}$, 020, 211, 300, $31\bar{1}$, 202 reflexions, in the same way described before. Results are shown in Table 13, in which cell-dimensions and cell-volumes of the raw specimens are inserted for comparison.

The results show that lattice contraction takes place by heating. In the specimen from Anag-ub, contraction takes place at 400°C and expansion at 800°C. This is likely to suggest that the specimen from Anag-ub is only slightly metamictized and by heating at about 400°C it reaches the maximum of contraction and by further heating begins to take place ordinary expansion.

Table 12. $\sin^2\theta$-values of the reflexions of heated specimens of allanite.

hkl	$\sin^2\theta$					
	From Anag-ub		From Omiya-chô (Morimoto)		From Kawamata-chô (Kojima)	
	400°C	800°C	400°C	800°C	400°C	800°C
001	.00716	.00711	.00701	.00712	.00703	.00708
100	.00912	.00908	.00911	.00906	.00911	.00911
$10\bar{1}$	.00935	.00929				
101	.02295	.02280	.02272	.02287	.02281	.02285
$10\bar{2}$	.02372	.02359				
011	.02519	.02496				
110	.02732	.02706	.02686	.02711	.02691	.02706
$\{11\bar{1}$ $\{002$	.02829	.02799				
$11\bar{2}$		.04158				.04137
012	.04661	.04610				.04623
$21\bar{1}$	.04809	.04809	.04770	.04770	.04783	.04783
210	.05462	.05438	.05382			.05462
201	.05703	.05664	.05688	.05746	.05717	.05717
$11\bar{3}$	.07054	.07023	.06980	.06964	.06991	.07023
020	.07246	.07215	.07204	.07231	.07172	.07172
211	.07508	.07475	.07461	.07475	.07475	.07535
300	.08180	.08128	.08100	.08145	.08100	.08128
$31\bar{1}$	.08714	.08679	.08661	.08661	.08597	.08697
202	.09145	.09108	.09078	.09157	.09126	.09211
$\{121$ $\{10\bar{4}$	.09530	.09499		.09376		.09499
$12\bar{2}$	.09616	.09585				
022	.10036	.10036	.09929	.10006		.10036
$\{22\bar{1}$ $\{31\bar{3}$	.10317	.10278	.10157			.10298
$22\bar{2}$	.10996	.10996	.10890	.10943		.10943

Table 12 (Cont.). $\sin^2\theta$-values of the reflexions of heated specimens of allanite.

hkl	$\sin^2\theta$					
	From Anag-ub		From Omiya-chô (Morimoto)		From Kawamata-chô (Kojima)	
	400°C	800°C	400°C	800°C	400°C	800°C
$\begin{cases}004\\11\bar{4}\end{cases}$	.11404	.11397		.11323		.11316
$\begin{cases}311\\40\bar{1}\end{cases}$	.12574	.12574	.12475	.12574		
221	.12902	.12902	.12824	.12882	.12836	.12881
$22\bar{3}$	.13197	.13177	.12996			
023	.13572	.13572		.13491		.13550
203		.13973		.13995		.14138
222	.16330	.16289				
312	.16785	.16785	.16605	.16782	.16612	.16693
$13\bar{2}$	.18862	.18853		.18846		
$23\bar{1}$	.19228	.19219				
303	.20530					
$13\bar{3}$	.21492	.21492	.21477	.21483	.21402	.21491
313	.22363	.22354	.22246	.22350	.22233	.22321

Table 13. Cell-dimensions and cell-volumes of raw and heated specimens of allanite.

		Raw specimen	Heated at 400°C	Heated at 800°C
From Anag-ub	*a*	8.929 Å	8.911	8.894
	b	5.736 Å	5.718	5.734
	c	10.147 Å	10.127	10.104
	β	114°54′	115°05′	114°32′
	V	471.41 Å^3	467.36	468.75
From Omiya-chô (Morimoto)	*a*	8.978 Å	8.937	8.945
	b	5.779 Å	5.736	5.730
	c	10.206 Å	10.172	10.191
	β	115°00′	115°00′	115°22′
	V	479.90 Å^3	472.57	471.97
From Kawamata-chô (Kojima)	*a*		8.951 Å	8.916
	b		5.749 Å	5.747
	c		10.145 Å	10.106
	β		115°08′	115°06′
	V		472.63 Å^3	468.93

3. Monazite

Specimens from Tôwa-mura (Harimichi), Fukushima Pref., Omiya-chô (Kôbe), Kyoto Pref. and India were submitted to the experiment. Diffraction patterns of the heated specimens together with those of the raw specimens are shown in Fig. 11, however, only in the range from 15° to 56° (2θ). As will be seen in Fig. 11,

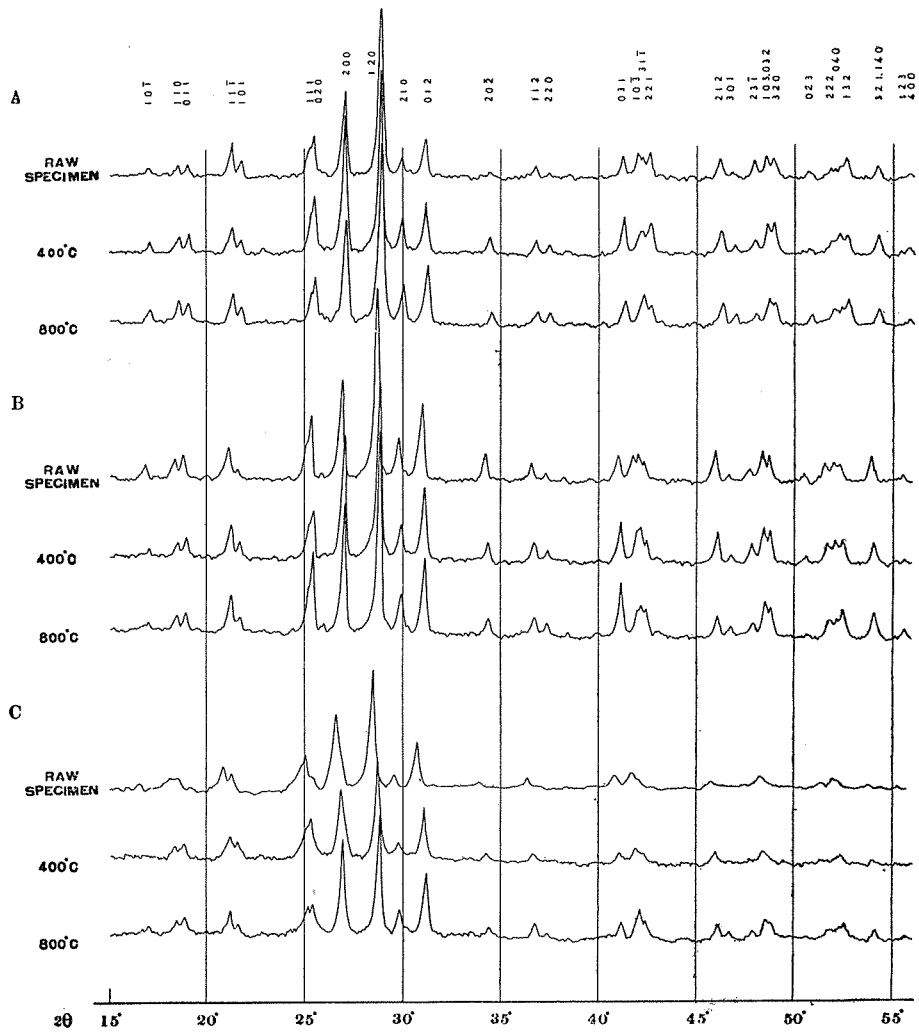

Fig. 11. Diffraction patterns of raw and heated specimens of monazite, showing the range from 15° to 56° (2θ). A. From Tôwa-mura (Harimichi). B. From Omiya-chô (Kôbe). C. From India.

the effect of heating on these specimens is considerable in shifting peaks towards high angle side, but not in increasing the sharpness and the height of the peaks.

In Table 14 are shown the $\sin^2\theta$–values of the reflexions of the heated specimens. Cell-dimensions and cell-volumes of the heated specimens were calculated from the $\sin^2\theta$–values, selecting 200, 120, 012, $20\bar{2}$, 112, 031, 212, 132 reflexions, in the same

Table 14. $\sin^2\theta$–values of the reflexions of heated specimens of monazite.

hkl	$\sin^2\theta$					
	From Tôwa-mura (Harimichi)		From Omiya-chô (Kôbe)		From India	
	400°C	800°C	400°C	800°C	400°C	800°C
$10\bar{1}$	.02193	.02193	.02176	.02184		.02202
110	.02582	.02592	.02582	.02592	.02547	.02576
011	.02716	.02732	.02716	.02726	.02706	.02706
$11\bar{1}$	.03404	.03415	.03404	.03415	.03393	.03404
101	.03534	.03553	.03542	.03549	.03534	.03542
111	.04809	.04809	.04757	.04770	.04722	.04770
020	.04858	.04858	.04844	.04858	.04822	.04844
200	.05476	.05490	.05462	.05471	.05410	.05452
120	.06225	.06240	.06200	.06220	.06185	.06255
210	.06713	.06713	.06672	.06693	.06641	.06682
012	.07247	.07263	.07156	.07204	.07204	.07247
$20\bar{2}$	.08779	.08809	.08744	.08744	.08726	.08779
112	.09998	.10017	.09929	.09948	.09891	.09948
220	.10330	.10349	.10298	.10298		.10278
031	.12454	.12475	.12376	.12433	.12341	.12397
$10\bar{3}$			.12824	.12845	.12824	.12924
$31\bar{1}$	.12996	.13039	.12938	.12960		
221	.13213	.13235	.13119	.13133	.13097	.13119
212	.15437	.15500	.15351	.15406	.15312	.15374
301	.15896	.15920	.15793	.15832		.15729
$23\bar{1}$	.16565	.16589	.16475	.16475		.16524
{103 / 032	.16974	.17024	.16867	.16892	.16851	.16958
320	.17223	.17198	.17090	.17090		.17090
023	.18378	.18447	.18310	.18310		
222	.19193	.19263	.19053	.19106		.19079
040	.19466	.19581	.19307	.19351		.19351
132	.19722	.19749	.19563	.19563	.19536	.19589
{321 / 140	.20821	.20867	.20684	.20703	.20639	.20657
123	.21940	.22015	.21846	.21865		

way described before. Results are shown in Table 15, in which cell-dimensions and cell-volumes of the raw specimens are inserted for comparison.

The results show that lattice contraction takes place by heating.

Table 15. Cell-dimensions and cell-volumes of raw and heated specimens of monazite.

		Raw specimen	Heated at 400°C	Heated at 800°C
From Tôwa-mura (Harimichi)	a	6.774 Å	6.782	6.773
	b	6.989 Å	6.984	7.002
	c	6.465 Å	6.453	6.435
	β	103°44′	103°43′	103°46′
	V	297.31 Å^3	296.92	296.40
From Omiya-chô (Kôbe)	a	6.809 Å	6.780	6.776
	b	7.030 Å	7.007	7.001
	c	6.511 Å	6.487	6.481
	β	103°47′	103°41′	103°44′
	V	302.68 Å^3	299.42	298.67
From India	a	6.845 Å	6.811	6.784
	b	7.033 Å	7.017	7.002
	c	6.513 Å	6.474	6.460
	β	104°00′	103°39′	103°34′
	V	304.23 Å^3	300.67	298.29

4. Xenotime

Specimen from Ishikawa-chô (Ishikawa), Fukushima Pref. was submitted to the experiment. Diffraction patterns of the heated specimens together with that of the raw specimen for comparison are shown in Fig. 12, however, only in the range from 16° to 56° (2θ). As will be seen in Fig. 12, the effect of heating comes in sight in increasing peaks in sharpness and in height, and in shifting them towards high angle side.

In Table 16 are shown the $\sin^2\theta$–values of the reflexions of the heated specimens. Cell-dimensions and cell-volumes were calculated from the $\sin^2\theta$–values in the same way described before. Results are shown in Table 17, in which cell-dimensions and cell-volume of the raw specimen are inserted for comparison.

The results show that lattice contraction takes place by heating.

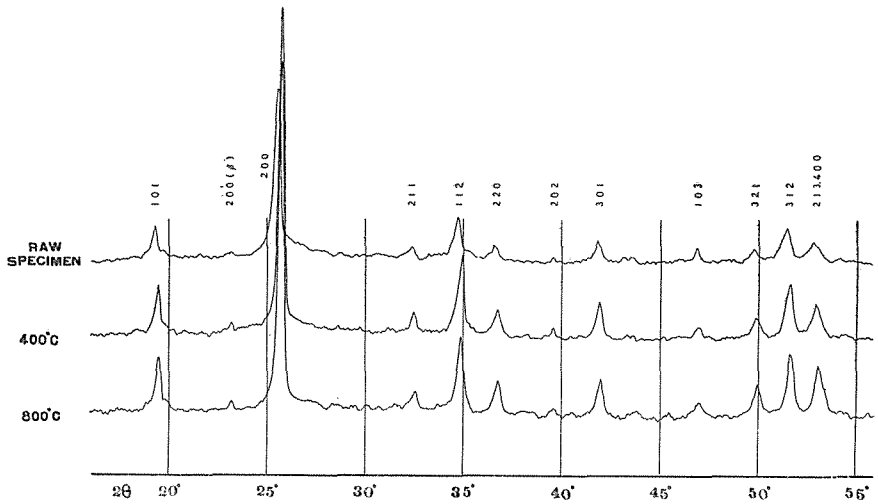

Fig. 12. Diffraction patterns of raw and heated specimens of xenotime, showing the range from 16° to 56° (2θ).

Table 16. $\sin^2\theta$-values of the reflexions of heated specimens of xenotime.

hkl	$\sin^2\theta$		*hkl*	$\sin^2\theta$	
	400°C	800°C		400°C	800°C
101	.02876	.02876	301	.12824	.12859
200	.04995	.04995	103	.15920	.15920
211	.07846	.07879	321	.17792	.17842
112	.09012	.09024	312	.18966	.18992
220	.09960	.09979	213 400	.19909	.19981
202	.11492	.11533			

Table 17. Cell-dimensions and cell-volumes of raw and heated specimens of xenotime.

	Raw specimen	Heated at 400°C	Heated at 800°C
a	6.882 Å	6.882	6.874
b	6.980 Å	6.958	6.943
c	6.120 Å	6.111	6.111
V	293.98 Å^3	292.62	291.65

5. Gadolinite

For the experiment, gadolinite from Arendal, Norway was the only specimen at the author's disposal. Diffraction pattern of the raw specimen together with those of the heated specimens are shown in Fig. 13, however, only in the range from 17° to 56° (2θ). As will be seen in Fig. 13, the effect of heating comes in sight in increasing peaks in sharpness and in height, and in shifting them towards high angle side. Indices of the reflexions were calculated making use of the result of structure analysis carried out by ITO and MORI (1953).

In Table 18 are shown the $\sin^2\theta$-values of the reflexions of the raw and the heated specimens. Cell-dimensions and cell-volumes were calculated from the $\sin^2\theta$-values, selecting 021, 013, 120, 031, 130, $13\bar{2}$, 040, 214 reflexions, by the following equation using the method of least squares.

$$4\sin^2\theta = h^2a^{*2}+k^2b^{*2}+l^2c^{*2}+2hla^*c^*\cos\beta^*$$

Results are shown in Table 19.

The results show that lattice contraction takes place by heating.

Table 18. $\sin^2\theta$-values of the reflexions of raw and heated specimens of gadolinite.

hkl	$\sin^2\theta$			*hkl*	$\sin^2\theta$		
	Raw specimen	Heated at 400°C	Heated at 800°C		Raw specimen	Heated at 400°C	Heated at 800°C
011		.01600	.01628	200	.10317	.10388	.10615
100	.02566	.02566	.02602	{210 032			.11792
012	.03280	.03364	.03415	130	.11896	.11944	.12131
{11$\bar{1}$ 111			.04252	11$\bar{4}$	.12960		.13352
021	.04679	.04683	.04770	13$\bar{2}$	.14198	.14236	.14478
10$\bar{2}$			.04986	22$\bar{1}$	.14977	.15000	.15249
11$\bar{2}$	.05910	.05919	.06032	221		.15101	.15327
112	.05978	.05988	.06086	040	.16484	.16500	.16826
013	.06255	.06295	.06426	{21$\bar{3}$ 22$\bar{2}$			.17156
120	.06672	.06713	.06817	{034 042		.18827	.19123
{12$\bar{1}$ 121	.07247	.07263	.07398	{22$\bar{3}$ 20$\bar{4}$			.20259
11$\bar{3}$	.08809	.08827	.09012	{223 204			.20521
113	.08928	.08958	.09108	231			.20986
031	.09791	.09791	.10017	214	.21151	.21224	.21557

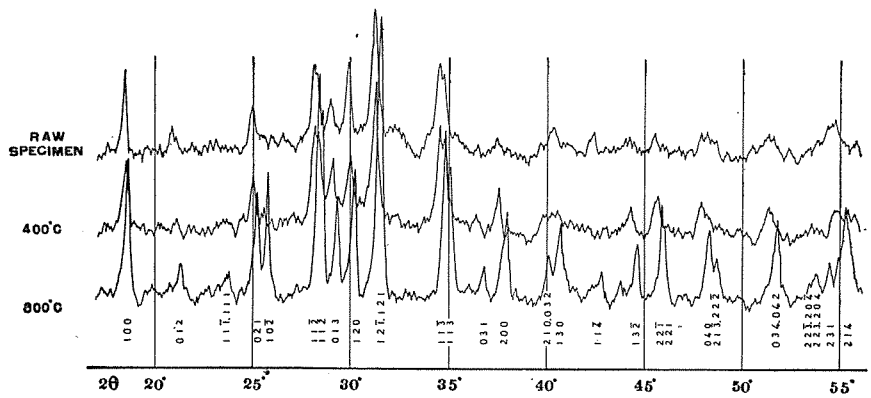

Fig. 13. Diffraction patterns of raw and heated specimens of gadolinite, showing the range from 17° to 56° (2θ).

Table 19. Cell-dimensions and cell-volumes of raw and heated specimens of gadolinite.

	Raw specimen	Heated at 400°C	Heated at 800°C
a	4.748 Å	4.726	4.724
b	7.595 Å	7.592	7.515
c	10.083 Å	10.062	9.948
β	90°44′	90°32′	90°46′
V	363.58 Å^3	360.98	353.11

IV. Melting and quenching radioactive minerals

It is desirable to carry out this experiment with non-metamict specimens. However, such specimens cannot be expected to be got easily. Therefore, specimens in a slight metamict state were submitted to the experiment. These specimens are as follows:

Allanite from Anag-ub, Whanghe-do, Korea
Gadolinite from Arendal, Norway
Zircon from Burma
Monazite from Ishikawa-chô (Nogizawa), Fukushima Pref.
Xenotime from Ishikawa-chô (Ishikawa), Fukushima Pref.

Pieces of the crystals of these minerals were kept separately in a crucible without cover, as large as 5 *cm* in diameter, made of Al_2O_3 together with Seger cones. The crucible was put into a furnace and heated on the outside by oxyacetylene flame. Temperature was measured by the Seger cones as well as by means of optical pyrometry. After the crucible was heated up to about 1800°C, it was taken out of

the furnace and quenched in air. In this treatment allanite and gadolinite melted completely and were absorbed into the crucible wall, while zircon, monazite and xenotime showed only a slight change in colour. Subsequently, experiment was carried out for each of the minerals individually with pieces of the same crystals in the same way, however, in the case of allanite and gadolinite a platinum crucible was used. Allanite melted at about 1400°C, gadolinite at about 1500°C, and zircon, monazite, xenotime showed the beginning of melting at about 1950°C (maximum resisting temperature of the furnace). The melts and the heated specimens were quenched in air and crushed into powders and then examined X-ray spectrometrically.

In order to get melts of zircon, monazite and xenotime, the following experiment was carried out. Cones which were about 10 *mm* in height and about 5 *mm* in diameter of base were made out of the specimens. They were stood in a mattress of alumina powders and were heated directly by oxyacetylene flame on the tops. In the case of monazite and xenotime, the top of the cone was melted by heating for about 15 minutes and drops of the melt dripped down on the surface of the cone. However, zircon, despite of prolonged heating, showed only the beginning of melting as in the case of heating at about 1950°C. The melts were quenched in air and crushed into powders and then examined X-ray spectrometrically.

1. Allanite

Diffraction pattern of the melt of allanite is shown in Fig. 14, together with that of the raw specimen for comparison, however, only in the range from 20° to 60° (2θ). As will be seen in Fig. 14, the former is quite different from the latter. In Table 20 are shown the $\sin\theta$-values and the intensities (heights of peaks) of the reflexions of the melt of allanite. The d-values, calculated from the $\sin\theta$-values, are also shown in Table 20. The melt is likely to consist of several phases, one of which is crystalline CeO_2. The d- and I-values of CeO_2 determined by SWANSON and TATGE (1953) are also inserted in Table 20 for comparison.

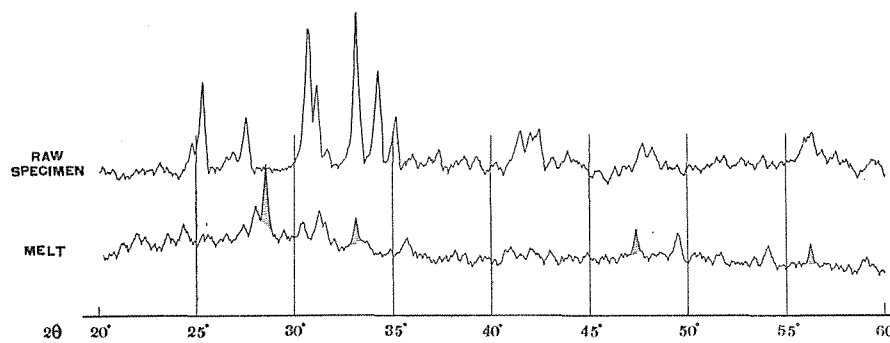

Fig. 14. Diffraction patterns of raw specimen and melt of allanite, showing the range from 20° to 60° (2θ). Shaded peaks are the reflexions of CeO_2.

Table 20. $\sin\theta$-values, d-values and intensities of the reflexions of melt of allanite and those of CeO_2.

Melt of allanite			CeO_2		Melt of allanite			CeO_2	
$\sin\theta$	d(Å)	I	d(Å)	I	$\sin\theta$	d(Å)	I	d(Å)	I
.1902	4.050	24			.2717	2.835	20		
.2102	3.664	30			.2849	2.704	40	2.706	29
.2368	3.253	24			.3062	2.516	24		
.2414	3.191	44			.4017	1.917	36	1.913	51
.2462	3.129	100	3.124	100	.4187	1.840	36		
.2540	3.032	16			.4558	1.690	24		
.2616	2.944	22			.4715	1.634	30	1.632	44
.2689	2.864	40							

2. Gadolinite

Diffraction pattern of the melt of gadolinite is shown in Fig. 15, together with that of the raw specimen for comparison, however, only in the range from 17° to 56° (2θ). As will be seen in Fig. 15, the former is quite different from the latter. In Table 21 are shown the $\sin\theta$-values and the intensities (heights of peaks) of the reflexions of the melt of gadolinite. The d-values, calculated from the $\sin\theta$-values, are also shown in Table 21. The melt is likely to consist of several phases, one of which is probably crystalline $Y_2O_3Fe_2O_3$. In Table 21 are also inserted the d- and I-values of $Y_2O_3Fe_2O_3$, which were introduced from the cards of the X-ray diffraction data (*A. S. T. M.*) for comparison.

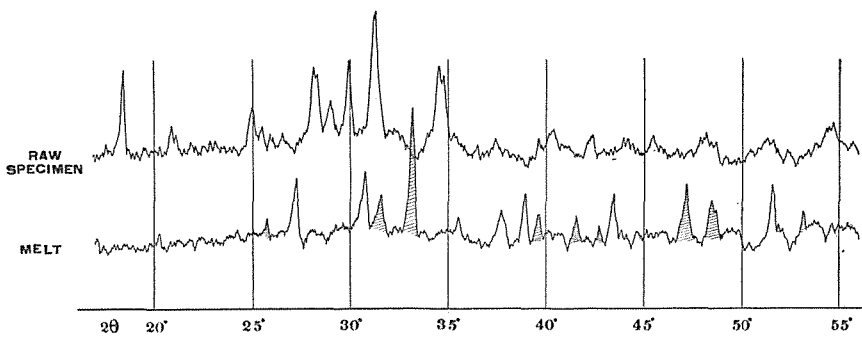

Fig. 15. Diffraction patterns of raw specimen and melt of gadolinite, showing the range from 17° to 56° (2θ). Shaded peaks are, probably, the reflexions of $Y_2O_3Fe_2O_3$.

Table 21. sin θ-values, d-values and intensities of the reflexions of melt of gadolinite and those of $Y_2O_3Fe_2O_3$.

Melt of gadolinite			$Y_2O_3Fe_2O_3$		Melt of gadolinite			$Y_2O_3Fe_2O_3$	
sin θ	d (Å)	I	d (Å)	I	sin θ	d (Å)	I	d (KX)	I
.1765	4.364	10			.3401	2.265	19	2.27	7
.2241	3.437	14	3.43	15	.3562	2.162	20	2.16	7(b)
.2363	3.260	48			.3651	2.110	15	2.11	10
.2661	2.895	48			.3714	2.074	40		
.2728	2.823	30	2.78	20	.4009	1.921	46	1.92	20
.2862	2.691	100	2.69	100	.4112	1.873	31	1.89	20
			2.62	30(b)	.4131	1.865	23	1.86	15(b)
.3060	2.517	14			.4358	1.767	46		
.3242	2.376	30			.4378	1.759	15	1.75	5
.3341	2.305	41			.4483	1.718	23	1.70	20

3. Zircon

Diffraction patterns of the specimens heated up to about 1800°C and about 1950°C are shown in Fig. 16, together with that of the raw specimen for comparison,

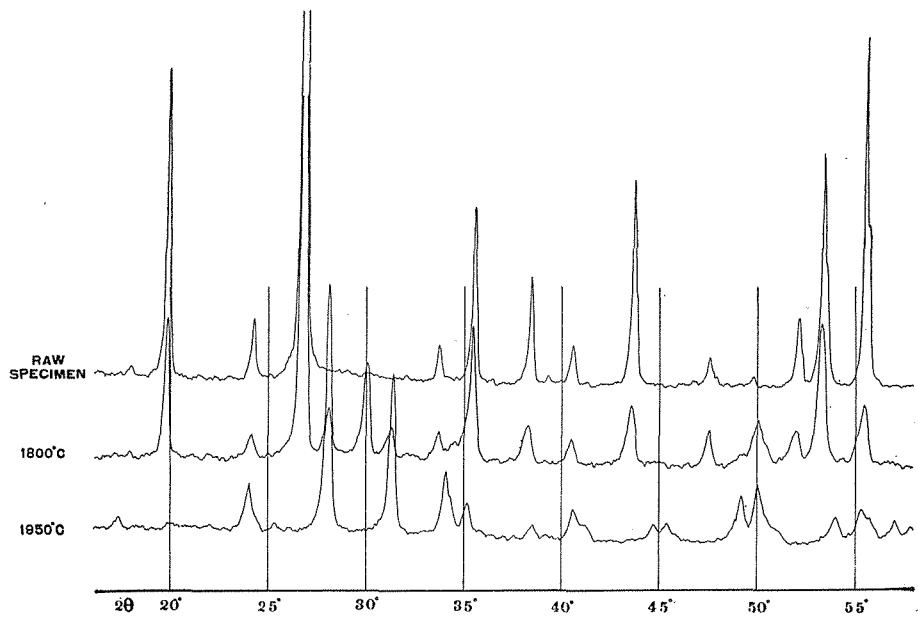

Fig. 16. Diffraction patterns of raw and heated specimens of zircon, showing the range from 16° to 58° (2θ).

however, only in the range from 16° to 58° (2θ). As will be seen in Fig. 16, the diffraction patterns are different from one another. In Table 22 are shown the $\sin\theta$-values and the intensities (heights of peaks) of the reflexions of the raw and

Table 22. $\sin\theta$-values, d-values and intensities of the reflexions of raw and heated specimens of zircon and those of baddeleyite.

Raw specimen			Heated to ca. 1800°C			Heated to ca. 1950°C			Baddeleyite	
$\sin\theta$	d (Å)	I	$\sin\theta$	d (Å)	I	$\sin\theta$	d (Å)	I	$d(KX)$	I
						.1513	5.091	5	5.1	5
.1739	4.429	40	.1734	4.442	37					
						.2090	3.685	19	3.69	24
.2332	3.303	100	.2323	3.316	100					
			.2431	3.168	11	.2431	3.168	100	3.19	100
			.2597	2.966	25					
			.2700	2.853	6	.2712	2.840	62	2.85	80
.2910	2.647	4	.2904	2.652	5					
						.2938	2.622	22	2.63	32
						.3029	2.543	10	2.55	16
.3060	2.517	23	.3054	2.522	35					
.3302	2.333	13	.3291	2.340	11	.3308	2.328	6	2.34	8
.3475	2.217	4	.3469	2.220	8					
						.3478	2.215	13	2.21	24
						.3527	2.184	6	2.20	7
.3733	2.063	25	.3716	2.073	15					
						.3813	2.020	6	2.01	16
						.3867	1.992	6	2.00	6
.4038	1.908	3	.4033	1.910	10					
						.4171	1.847	17	1.85	32
			.4234	1.819	10	.4237	1.818	24	1.81	40
.4402	1.750	8	.4392	1.754	8					
.4501	1.711	30	.4491	1.715	34					
						.4545	1.695	10	1.70	20
						.4651	1.656	11	1.66	24
.4669	1.650	43	.4659	1.653	11					
						.4684	1.644	7	1.62	5

the heated specimens of zircon. The d-values calculated from the $\sin\theta$-values are also shown in Table 22. The d- and I-values of baddeleyite (ZrO_2), which are introduced from the cards of the X-ray diffraction data (*A. S. T. M.*), are also inserted in Table 22 for comparison.

Comparing these values with one another, it follows that in zircon heated to about 1800°C there are three sorts of crystalline phase, two of them are zircon and baddeleyite, and in zircon heated to about 1950°C there is one crystalline phase, that is, baddeleyite. Therefore, zircon begins to take place decomposition at about 1800°C.

4. Monazite

Diffraction patterns of the specimens heated up to about 1800°C and about 1950°C and the melt are shown in Fig. 17, together with that of the raw specimen for comparison, however, only in the range from 15° to 56° (2θ). As will be seen in Fig. 17, the diffraction patterns of the raw and the heated specimens are almost the same. However, the diffraction pattern of the melt makes a little difference from those of the others. In Table 23 are shown the $\sin\theta$–values and the intensities (heights of peaks) of the reflexions of the raw and the heated specimens and the melt. In Table 23 are also inserted the d–values of the melt, calculated from the $\sin\theta$–values, and the d– and I–values of thorianite (ThO_2) determined by SWANSON and TATGE (1953) for comparison.

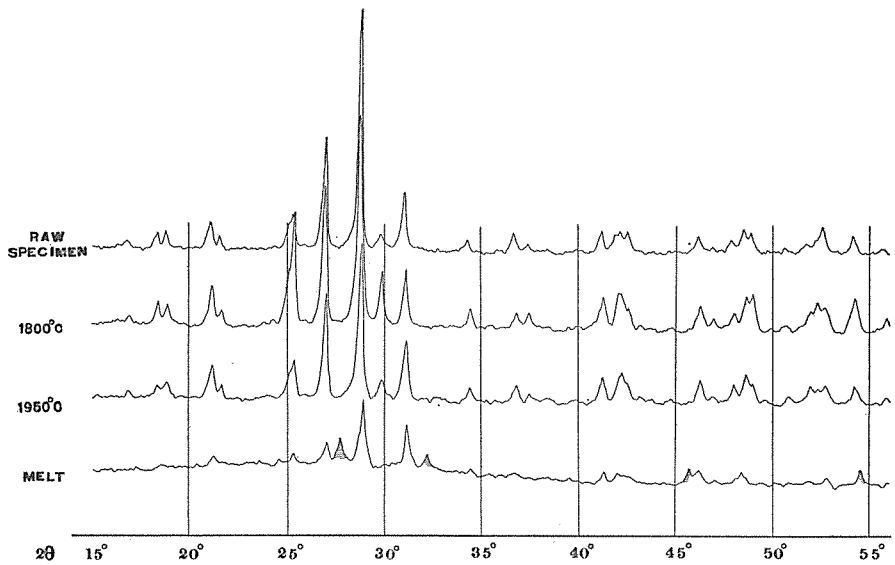

Fig. 17. Diffraction patterns of raw and heated specimens and melt of monazite, showing the range from 15° to 56° (2θ). Shaded peaks are the reflexions of ThO_2.

Evidently, in the melt of monazite there are two sorts of crystalline phase, that is, monazite and thorianite. Specimen submitted to the present experiment contains 10.01% of ThO_2 as described before. If such impurity were not contained, only crystalline monazite would appear in the melt of monazite.

Table 23. $\sin\theta$-values and intensities of the reflexions of raw and heated specimens and melt of monazite. d-values and intensities of the reflexions of thorianite.

Raw specimen		Heated to ca. 1800°C		Heated to ca. 1950°C		Melt			Thorianite	
$\sin\theta$	I	$\sin\theta$	I	$\sin\theta$	I	$\sin\theta$	d (Å)	I	d (Å)	I
.1474	3	.1487	3	.1481	5					
.1607	9	.1613	7	.1607	8					
.1645	10	.1653	6	.1653	10					
.1842	21	.1851	11	.1854	22	.1847		17		
.1882	12	.1891	4	.1890	8					
.2184	18	.2195	16	.2196	18					
.2201	26	.2210	35	.2210	15	.2193		17		
.2340	50	.2349	60	.2349	67	.2343		29		
						.2388	3.226	38	3.234	100
.2493	100	.2501	100	.2501	100	.2498		100		
.2585	12	.2594	15	.2594	13					
.2684	41	.2695	15	.2700	37	.2686		60		
						.2776	2.775	17	2.800	35
.2954	9	.2971	6	.2971	8	.2957		10		
.3154	15	.3168	4	.3168	10					
.3212	6	.3220	4	.3223	3					
.3524	15	.3532	10	.3532	15	.3529		17		
.3581	12	.3600	21	.3605	16	.3586		12		
.3600	14	.3614	10	.3614	18	.3614		11		
.3630	13	.3641	6	.3638	8	.3633		8		
						.3881	1.985	23	1.980	58
.3921	12	.3937	8	.3937	13	.3923		21		
.3979	3	.3995	3	.3990	3					
.4059	9	.4078	4	.4073	11					
.4110	13	.4128	10	.4128	18	.4099		17		
.4144	12	.4158	11	.4155	11					
.4276	4	.4295	2	.4300	5					
.4365	5	.4389	5	.4386	10					
.4402	10	.4418	6	.4418	8					
.4428	14	.4444	8	.4446	10	.4441		13		
.4555	12	.4568	11	.4566	10					
						.4574	1.684	24	1.689	64
.4667	3									
.4677	3	.4692	3	.4692	4					

5. Xenotime

Diffraction patterns of the specimens heated up to about 1800°C and about 1950°C and the melt are shown in Fig. 18, together with that of the raw specimen for comparison, however, only in the range from 16° to 56° (2θ). As will be seen in Fig. 18, the diffraction patterns are much the same. In Table 24 are shown the

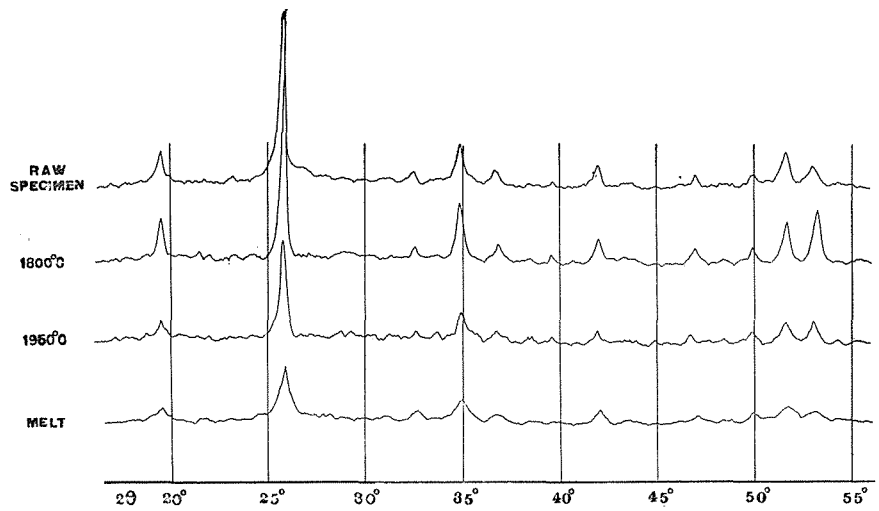

Fig. 18. Diffraction patterns of raw and heated specimens and melt of xenotime, showing the range from 16° to 56° (2θ).

Table 24. $\sin\theta$-values and intensities of the reflexions of raw and heated specimens and melt of xenotime.

Raw specimen		Heated to ca. 1800°C		Heated to ca. 1950°C		Melt	
$\sin\theta$	I	$\sin\theta$	I	$\sin\theta$	I	$\sin\theta$	I
.1691	19	.1696	19	.1696	16	.1691	20
.2233	100	.2235	100	.2235	100	.2235	100
.2801	7	.2804	6	.2807	7	.2807	17
.2996	21	.2996	28	.2999	24	.2999	34
.3145	10	.3162	8	.3159	9	.3151	11
.3390	2	.3385	4	.3387	4		
.3581	12	.3586	13	.3584	10	.3586	20
.3987	7	.3990	6	.3982	7	.3993	11
.4218	7	.4221	9	.4221	9	.4216	17
.4350	17	.4358	21	.4358	18	.4350	31
.4462	10	.4483	28	.4475	18	.4467	20

$\sin\theta$-values and the intensities (heights of peaks) of the reflexions of the raw and the heated specimens and the melt. In the melt of xenotime there is only a crystalline phase, that is, xenotime.

Now, it has been clarified that the melts of monazite and xenotime solidify in their original crystalline phases even by the quenching under the ordinary pressure, while the melts of allanite and gadolinite do not. In the present experiment melt of zircon has not been obtained, nevertheless, no observation of the original crystalline phase in zircon heated to about 1950°C and quenched in air suggests that zircon does not recrystallize to its original crystalline phase.

V. Discussion

There are two sorts of radioactive minerals, one is that which is transformed into an amorphous state retaining crystal form, the other is that which is always in a crystalline state. The author has given an opinion for the arising of this phenomenon in the 2nd section. That is, summarizing, as follows: In the former, some portion of the crystal may distend by the production of interstitials and vacancies and other portion may melt by the generation of heat, which are caused by the irradiation accompanied with disintegration of the radioactive elements contained in the crystal. The melted portion may take place decomposition, and whether the decomposed portion may solidify in crystalline phase (or phases) or in amorphous phase by quenching, the mineral may become amorphous optically as well as X-ray spectrometrically as the decomposed portions increase, owing to that the newly formed crystals may be extremely minute and may be randomly orientated. While in the latter, although some portion may distend by the production of interstitials and vacancies and other portion may melt by the generation of heat as in the case of the former, the melted portion may not take place decomposition and may solidify in the original crystalline phase by quenching and, therefore, the mineral may not become amorphous.

In order to accept this opinion as a true nature of the metamictization, it is necessary to be proved, as said before, that the same crystalline phase precipitate in melting and then quenching radioactive minerals which are always crystalline, and amorphous phase or crystalline phase (or phases) other than the original one in so doing radioactive minerals which are usually amorphous; and that lattice contraction takes place in heating radioactive minerals in which metamictization is in progress. These necessary conditions were satisfactorily proved in the present experiments.

Production of interstitials and vacancies and generation of heat will be mainly due to the energies of alpha rays and recoil atoms. Beta rays and gamma rays may not play a effective role in this process on account of their far lower energies, compared with those of alpha rays and recoil atoms.

As is well known, the average energy of an alpha-particle in uranium and actinouranium series is of the order of magnitude of 5.5×10^6 ev, in thorium series

of the order of magnitude of 6.0×10^6 ev and the energy of a recoil atom is of the order of magnitude of 10^5 ev, on the other hand, atoms in a crystal are held in their lattice sites with energy of about 5 ev or more, and the energy needed to displace an atom in a crystal from its lattice site is in the neighbourhood of 25 ev. According to SLATER (1951), however, about 99% of the energy of alpha-particle is dissipated through the excitation of electronic system, and the remaining energy through the atomic collisions, producing interstitials and vacancies and generating heat, while the greater part of the energy of recoil atom is dissipated by the atomic collisions, producing interstitials and vacancies and generating heat.

Apart from that, if the energy passed on to an atom is reduced to 1 ev or less by interchange with its neighbours so that about 10^5 such atoms are involved, macroscopic concepts of heat will be possible to be applied, and the temperature of the portions bombarded by alpha-particle or knocked by recoil atom will rise to more than the melting points of crystals. Therefore, the melting by the bombarding of alpha-particle or by the knocking of recoil atom and the quenching which follows the melting will bring about the same result which arise at the time when a crystal is heated up to above its melting point and then quenched. The difference between these two is that in the former melting and quenching are limited to extremely small portions within a crystal, while in the latter they extend simultaneously over all the portions of a crystal. Consequently, in the case of the former even if the newly formed phases may be crystalline they may be so minute in size as to fail in an X-ray diffractometry.

Besides monazite and xenotime, there are two more radioactive minerals which have not been found in a metamict state, that is, thorianite and huttonite as said before. In the present study these minerals have not been submitted to the experiment owing to the lack of the specimens. However, as stated before, in the melt of monazite which contained 10.01% of ThO_2 two sorts of crystalline phase, that is, monazite and thorianite were precipitated; and according to PABST (1952), huttonite heated to about 1400°C showed no change upon the X-ray photograph, almost fully metamict thorite heated at 1000°C for 15 hours and that heated at about 1400°C for the same period gave huttonite patterns, other five metamict specimens of thorite heated below 1200°C for from 1 to 140 hours gave the patterns of thorite, huttonite and thorianite, but the same specimens heated at above 715°C for prolonged hours and at about 1400°C for 15 hours gave huttonite patterns with trace of thorianite patterns. These experimental results may suggest that thorianite and huttonite also crystallize to their original crystalline phases respectively when they were melted and then quenched.

Lastly, the author must relate to uraninite. The mineral can be easily prepared in a laboratory, none the less, it is sometimes transformed into a disordered state. According to HURLEY and FAIRBAIRN (1953), the disordering of uraninite is another thing, although it bears a striking resemblance to the metamictization in appearance. They attributed the disordering of the mineral to oxidation. Their conclusion has been derived from the results of the works made by KATZ and RABINOWITCH (1951)

and BROOKER and NUFFIELD (1951). The author is in agreement with HURLEY and FAIRBAIRN.

Acknowledgment

The author wishes to express his sincere thanks to Dr. T. ITO who kindly gave him advice in this work. He also expresses his hearty gratitude to Doctors J. MAKIYAMA, S. MATSUSHITA, N. KUMAGAI and A. HARUMOTO for their encouragements. He is also indebted to the Norelco Administration Committee in Tokyo University for the permission to use its Norelco Geiger counter X-ray spectrometer. He is especially grateful to Dr. B. YOSHIKI who afforded facilities in melting minerals. He is also thankful to Doctors K. OMORI, K. SAKURAI and J. SHANKAR who sent him valuable specimens for the present experiments.

A part of this study was made by the financial aid of the Scientific Research Expenditure of the Ministry of Education, to which is due the author's gratitude.

References

BAUER, A. (1939): Untersuchungen zur Kenntnis der spezifisch leichten Zirkone; Neu. Jahr. Min. Geol. Palä., Beilage-Bände, A, **75**, 159.

BRINKMAN, J. A. (1954): On the nature of radiation damage in metals; Jour. Appl. Phys., **25**, 961.

BROOKER, E. J. and NUFFIELD, E. W. (1951): Studies of radioactive compounds (IV). Pitchblende from Lake Athabaska; Bull. Geol. Soc. Am., **62**, 1425.

FAESSLER, A. (1942): Untersuchungen zum Problem des metamikten Zustandes; Zeit. Krist., **104**, 81.

HOLLAND, H. D. and GOTTFRIED, D. (1955): The effect of nuclear radiation on the structure of zircon; Acta Cryst., **8**, 291.

HURLEY, P. M. and FAIRBAIRN, H. W. (1953): Radiation damage in zircon, a possible age method; Bull. Geol. Soc. Am., **64**, 659.

HUTTON, C. O. (1950): Studies of heavy detrital minerals; Bull. Geol. Soc. Am., **61**, 635.

ITO, T. and MORI, H. (1953): The crystal structure of datolite; Appendix, On the structure of gadolinite; Acta Cryst., **6**, 31.

KARKHANAVALA, M. D. and SHANKAR, J. (1954): An X-ray study of natural monazite; Proc. Indian Acad. Sci., **40**, 67.

KATZ, J. J. and RABINOWITCH, E. (1951): The chemistry of uranium (I). The element, its binary and related compounds; Nat. Nuclear Energy Ser. XII, 5. New York.

KINCHIN, G. H. and PEASE, R. S. (1955): The displacement of atoms in solids by radiation; Rep. Prog. Phys., **18**, 1.

MÜGGE, O. (1922): Über isotrop gewordene Kristalle; Cbl. Min. Geol. Palä., 721 und 753.

PABST, A. (1951): Huttonite, a new monoclinic thorium silicate; Am. Min., **36**, 60.

PABST, A. (1952): The metamict state; Am. Min., **37**, 137.

SEITZ, F. (1949): On the disordering of solids by action of fast massive particles; Disc. Fara. Soc., **5**, 271.

SLATER, J. C. (1951): Effects of radiation on materials; Jour. Appl. Phys., **22**, 237.

SWANSON, H. E. and TATGE, E. (1953): Standard X-ray diffraction powder patterns (I); National Bureau of Standards Circular, 539.

UEDA, T. (1953): The crystal structure of monazite ($CePO_4$); Memoirs Coll. Sci. Univ. Kyoto, B, **20**, 227.

UEDA, T. and KOREKAWA, M. (1954): On the metamictization; Memoirs Coll. Sci. Univ. Kyoto, B, **21**, 151.

UEDA, T. (1955): The crystal structure of allanite, $OH(Ca, Ce)_2(Fe^{III}, Fe^{II})Al_2OSi_2O_7SiO_4$; Memoirs Coll. Sci. Univ. Kyoto, B, **22**, 145.

UEDA, T. and KOREKAWA, M. (1955): X-ray measurement of the lattice destruction and its recovery on some radioactive minerals; Mineralogical Jour., **1**, 198.

VEGARD, L. (1926): Results of crystal analysis; Phil. Mag. (7), **1**, 1151.

VEGARD, L. (1927): The structure of xenotime and the relation between chemical constitution and crystal structure; Phil. Mag. (7), **4**, 511.

VON STACKELBERG, M. und CHUDOBA, K. (1937): Dichte und Struktur des Zirkons (II); Zeit. Krist., **97**, 252.